AN ALL-PRESSURE FLUID-DROP MODEL: VALIDATION AND SPECIES SYSTEM DEPENDENCY

J. Bellan and K. Harstad
Jet Propulsion Laboratory
California Institute of Technology
Pasadena, CA 91109-8099

Abstract

A fundamental and very general model of fluid drop behavior at all pressures is presented and is shown to reproduce microgravity experimental data for heptane drops in nitrogen. In the model, the existence of a drop surface (i.e. phase discontinuity) is not necessarily assumed. The optical drop diameter is defined as the location of the maximum density-gradient magnitude. An examination of the drop-diameter-squared variation with time for the heptane/nitrogen system shows that it is approximately linear only at atmospheric pressure and has a negative curvature at higher pressures. As the pressure increases, the slope of the diameter squared becomes an increasing function of time and progressively increases with pressure at subcritical far-field temperatures, however, at supercritical temperatures a maximum is reached. A similar investigation conducted for oxygen drops in hydrogen reveals that at higher then atmospheric pressure the slope of the diameter squared versus time has a positive curvature. Given that the drop diameter squared versus time exhibits different behavior with pressure for the two species systems, it is concluded that high-pressure behavior should not be extrapolated from one species system to another. The results also show that, independent of the species system, at locations arbitrarily near the boundary, the drop does not reach the mixture critical point within the range of conditions investigated. An examination of the relaxation time at the drop boundary shows that quasi-steadiness of the mass transfer prevails even for relatively small drops. On an appropriate scale, the slope of the diameter squared versus time is shown to be independent of the drop size at all pressures.

1 INTRODUCTION

The study of drop behavior in high pressure environments has been of interest for many decades owing to its relevance to costly combustion devices such as gas turbine and liquid rocket engines. Since high pressure tests are expensive and sometimes dangerous, considerable effort has been devoted to the development of accurate models capable of simulating drop evolution at all pressures. A recent review by Bellan[1] tabulates current drop models published over more than a decade. Although most models are based on the transient conservation equations augmented by the real gas equation of state (EOS), and include thermodynamic-variable-dependent transport properties, the overwhelming majority of these models contains simplifying assumptions meant to enable less computationally intensive simulations. Such common assumptions are the existence of a drop surface assumed to be at an existing critical locus[2–5] or assumed to be at an existing location of mass flux quasi-steadiness, sometimes called thermodynamic equilibrium[2,5–12], and the neglect of the thermal diffusion effects represented by the Soret and Dufour term for the species and energy equations, respectively. Predictions from such models include, for example, the validity of the linear diameter squared, d^2, variation with time even at high pressures (e.g. Yang et al.[3] for the LOX/H_2 system); if such results were correct, it would enable a considerable simplification in the incorporation of drop models in complex Computational Fluid Dynamics (CFD) codes. Therefore, there is an incentive to examine the set of physical ingredients necessary to achieve agreement with data, as well as to determine possible simplifications that may result in large reductions of computational costs.

Approved for public release, distribution is unlimited. Copyright © 2002 by the California Institute of Technology. All rights reserved.

In this paper we summarize and conceptually integrate the investigations of Harstad and Bellan[13–15] in order to develop a perspective on the behavior of fluid drops for two different binary species systems. We first present the highlights of the very general model developed[13] and build confidence in its realism by showing that it has been validated with the microgravity experimental data of Nomura et al.[16] , which is for the heptane/nitrogen system. We also apply the same model to the study of the LOX/H_2 system and discuss both similarities and differences in behavior between the two species systems. Then, we systematically discuss the timewise variation of d^2 for isolated drops as a function of pressure for both moderate and elevated surrounding-fluid temperatures[14] . Finally, we evaluate the assumptions imposed on the drop boundary, that is the existence of a discontinuity that may be a surface, the possibility that the critical mixture point is reached arbitrarily near it, or that it may be in a quasi-steady mass-flux state (i.e. the value of the flux of molecules leaving the boundary is very nearly equal to that of molecules arriving at the boundary). A discussion of the impact of these results on future work is presented in the Conclusions.

2 CONSERVATION EQUATIONS

The model equations for an isolated, spherical drop have been previously developed by Harstad and Bellan[13] . To avoid undue repetition of published material, only the highlights and final conservation equations are given herein, and the reader is referred to that publication for details on this model.

The fundamental base of the model is Keizer's fluctuation-dissipation (FD) theory[17] , which formally accounts for non-equilibrium processes and furthermore naturally relates fluxes and forces for a general fluid by providing the form of the transport matrix. According to FD theory, the general flux equations are given by additive forms whereby both the molar fluxes, $\mathbf{J}_\alpha$, with α denoting the species, and the heat flux, $\mathbf{q}$, are the sums of coefficients multiplied by ∇X_β with $\beta \in [1, N_{sp}]$, X being the molar fraction and N_{sp} being the total number of species, of a coefficient multiplied by ∇T, where T is the temperature, and of a coefficient multiplied by ∇p, where p is the pressure. These matrix coefficients are functions of thermodynamic quantities and transport coefficients[13] . Note that, the general form of the transport matrix includes, additional to the well known Fick mass diffusion and Fourier heat conduction terms, the Soret term in the molar flux and the Dufour term in the heat flux. For a binary set of species, these new terms are proportional to a single new transport coefficient, the thermal diffusion factor. For a multispecies system, a set of thermal diffusion factors is involved.

2.1 GOVERNING EQUATIONS

According to Harstad and Bellan[13] , the isolated drop conservation equations are:

$$\frac{\partial \rho}{\partial t} + \frac{1}{r^2}\frac{\partial (r^2 \rho u)}{\partial r} = 0, \tag{1}$$

$$\frac{\partial (\rho u)}{\partial t} + \frac{1}{r^2}\frac{\partial (r^2 \rho u u)}{\partial r} + \frac{\partial p}{\partial r} = \frac{\partial \tau_{rr}}{\partial r} + \frac{3\tau_{rr}}{r}, \tag{2}$$

$$\rho \frac{DY_j}{Dt} = -m_j \nabla \cdot \vec{J}_j, \tag{3}$$

$$nC_p \frac{DT}{Dt} = \alpha_v T \frac{Dp}{Dt} - \nabla \cdot \vec{q} + \Phi_v + \sum_{l=1}^{N_{sp}} (h_l \nabla \cdot \vec{J}_l), \tag{4}$$

representing the continuity and the momentum, species and energy conservation. In these equations, ρ is the mass density; u is the radial velocity; r is the radial coordinate; $\tau_{rr} = (4/3)\eta[\partial u/\partial r - u/r]$ is the stress tensor; η is the mixture viscosity; Y_j is the mass fraction of species j; m_j is the molar mass; n is the molar density; C_p is the mixture molar heat capacity at constant pressure; $h_j = (\partial h/\partial X_j)_{p,T,X_{l\neq j}}$ is the partial

molar enthalpy where h is the total molar enthalpy; $\alpha_v = [(\partial v/\partial T)_{p,X_i}]/v$ is the thermal expansion ratio with v being the molar volume; $\Phi_v = (4/3)\eta[\partial u/\partial r - u/r]^2$ is the viscous dissipation and $D/Dt \equiv \partial/\partial t + u(\partial/\partial r)$. For a binary species mixture (species subscripts 1 and 2 with $m_1 > m_2$), the fluxes can be written in compact form as related to the transport matrix

$$\begin{pmatrix} -J_{1r} \\ -q_r \end{pmatrix} = \begin{pmatrix} A_J & B_J & C_J \\ C_q & A_q & B_q \end{pmatrix} \begin{pmatrix} \frac{\partial Y_1}{\partial r} \\ \frac{\partial T}{\partial r} \\ \frac{\partial p}{\partial r} \end{pmatrix} \tag{5}$$

where $-J_{1r}$ and $-q_r$ are the radial fluxes and

$$A_J = (m/m_1)nD\alpha_D, \quad B_J = (m_2/m)nDX_1X_2(\alpha_{IK} - \alpha_h)/T \tag{6}$$

$$C_J = (m_2/m)nD(m_1m_2X_1X_2/m)(v_1/m_1 - v_2/m_2)/(R_uT) \tag{7}$$

$$A_q = \lambda + (\alpha_{IK} - \alpha_h)\alpha_{IK}R_unDX_1X_2, \quad B_q = nD\ \alpha_{IK}(m_1m_2X_1X_2/m)(v_1/m_1 - v_2/m_2) \tag{8}$$

$$C_q = [m^2/(m_1m_2)]nD\ \alpha_D\alpha_{IK}R_uT \tag{9}$$

where $m = X_1m_1 + X_2m_2$ is the mixture molar mass, R_u is the universal gas constant, λ is the thermal conductivity, α_{IK} is the Irwing-Kirkwood form of the thermal diffusion factor (see Harstad and Bellan[13]), and D is the mixture diffusivity.

The binary mass diffusion factor can be calculated from thermodynamics

$$\alpha_D = 1 + X_1\partial \ln \gamma_1/\partial X_1 \tag{10}$$

where $\gamma_1 \equiv \varphi_1/\varphi_1^o$ is the activity coefficient and φ is the fugacity coefficient with the superscript o denoting the pure ($X_1 = 1$) limit. According to Harstad and Bellan[13] , the Bearman-Kirkwood form of the thermal diffusion factor, α_{BK}, is related to α_{IK} by

$$\alpha_{BK} = \alpha_{IK} - \alpha_h, \quad \alpha_h \equiv (m_1m_2/m)(h_1/m_1 - h_2/m_2)/(R_uT). \tag{11}$$

These two factors correspond to the two forms of the heat flux vector (see Sarman and Evans[18]). In the above derivation (c.f. eq. 8), it has been carefully ensured that the expression for the thermal conductivity converges to the kinetic value in the low pressure limit[13] , and thus that its value is indeed that tabulated or calculated through corresponding states procedures[19] .

To close the system of equations, the real gas EOS presented by Harstad et al.[20] is coupled to the above system of differential equations.

2.2 BOUNDARY CONDITIONS

The above conservation equations pertain to the entire field, $0 \leq r \leq R^{si}$, where R^{si} is the instantaneous location of the far field boundary, which is initially specified and is further calculated in a Lagrangian manner as part of the solution (see below). The far-field (subscript e) and drop-boundary conditions are those derived in Harstad and Bellan[13] , and the reader is referred to that publication for the detailed derivation.

Several aspects of these boundary conditions are noteworthy. At $r = R^{si}$, the values of the thermodynamic variables are specified (they can be either constant or functions of time). At the drop boundary, the conservation statements are stated as jump conditions across the boundary, relating locations within (R_d^-) and outside (R_d^+) the drop; that is, the drop boundary is treated as a mathematical discontinuity. Within the context of this study relying on thermodynamic concepts, this is the only physically, and therefore mathematically sound approach since in the layer between R_d^- and R_d^+, usual thermodynamic concepts do not apply because the molecular forces in the layer are not homogeneous as the molecular distribution is inhomogeneous. This emphasizes the fact that one cannot assume the state of the drop boundary, unless

corroborated by molecular dynamics (MD) calculations resolving the details of the layer, whereby the conditions at R_d^- and R_d^+ are imposed, and the MD obtained solution determines the structure of the boundary layer at R_d. We distinguish between the Lagrangian location of the initial drop boundary, R_d^0, which is followed in time, $R_d(t)$, and the location of the 'optical' drop boundary (not necessarily an interface), $R_s(t)$, which is also followed in time being calculated *a posteriori* of the solution as the location of the largest density change. The largest density change corresponds to either the location of the largest density gradient, or a density jump as it is an infinite gradient which is not calculable. This definition is relevant to optical observations, which identify changes in the index of refraction. Of importance is the fact that we do not assume the existence of a material interface in the region $0 \leq r \leq R^{si}$. If such an interface exists at any time, it is totally consistent with our definition whereby the drop boundary is identified to be at the location of the largest density change, $r = R_s$. Just as important, consistent with the discussion above noting that no assumption can be made regarding the state of the drop boundary, we do not assume phase equilibrium anywhere in the computational domain, and we do not necessarily relate the critical point of the mixture to any of the radial locations in the flow. This very general formulation makes the model ideally suited for evaluating assumptions about the state of the drop arbitrarily near the boundary, that is about the states at R_d^- and R_d^+ since within the formalism of the mathematical discontinuity, only the location of R_d is known and the conditions at R_d are not defined.

3 MIXTURE CRITICAL POINT

According to Peng and Robinson[21] , the critical point occurs when both the determinant of the second derivatives, $\mid \overline{\overline{U}} \mid$ (i.e. $U_{ij} = \partial^2 G/\partial X_i \partial X_j$), of the Gibbs function, G, and that of the second derivatives of G combined with the first derivatives of $\mid \overline{\overline{U}} \mid$ are null. Therefore, the accuracy of mixture critical point calculations is highly dependent of the accuracy of the EOSs. To verify the reliability of the present mixture critical locus, comparisons of critical locus calculations were performed based upon both the Peng-Robinson definition[21] and the free energy method of Reid et al.[19] , and they were further compared to data for two binary species systems. Thus, calculations for decane/CO_2 and for ethane/heptane were compared with the data of Reamer and Sage[22] and Kay[23] , respectively. For both binary mixtures, the computational results using the two methods agreed and duplicated the data with very good accuracy (not shown).

A consequence of the definition of the critical point is the fact that a necessary condition for attaining the binary mixture critical point is that the mass diffusion factors, α_{Dij}, be null since for a multicomponent system

$$\alpha_{Dij} \equiv [1/(R_u T)][X_i \partial \mu_i / \partial X_j] = [1/(R_u T)][X_i (\partial^2 G/\partial X_i \partial X_j)_{p,T,X_k}] \tag{12}$$

where μ is the chemical potential. According to the Gibbs-Duhem relationship, for a binary mixture there is a single value of the mass diffusion factor, $\alpha_D = \alpha_{D11} = \alpha_{D22} = -\alpha_{D12} = -\alpha_{D21}$. This observation is of significance since for a binary species system the single value of α_D can serve as 'diagnostic' to determine whether the critical point has been reached. That is, $0 < \alpha_D < 1$, with the null value corresponding to a possible critical point and the unity value corresponding to the ideal mixture state. This information can further support the evidence provided by the values of the reduced pressure, $p_r = p/p_c$, and reduced temperature, $T_r = T/T_c$, where the subscript 'c' denotes the critical point.

4 RESULTS

The numerical method used to solve the equations has been detailed elsewhere[13] and will not be repeated here. Simulations were conducted for heptane ($T_c = 540.3$ K, $p_c = 2.76$ MPa) drops in nitrogen ($T_c = 126.2$ K, $p_c = 3.39$ MPa), and for oxygen ($T_c = 154.6$ K, $p_c = 5.043$ MPa) drops in hydrogen ($T_c = 33.2$ K, $p_c = 1.313$ MPa). The kinetic law governing the molecular motion to and from the drop boundary is

$$F_{ems} = \sum_{j=1,2} [\alpha_{aj} m_j u_{Tj} (n_{j,equil}^G - n_j^G)], \tag{13}$$

where α_{a1} and α_{a2} represent the accommodation coefficients, $F_{ems} \equiv -(1/A_d) dM/dt$ (M is the drop mass and A_d is the drop boundary area) is the mass 'emission' rate from the drop boundary corresponding to

the evaporation rate at atmospheric pressure, $n^G_{j,equil}$'s are calculated (superscript G indicates the initial nitrogen or hydrogen side of the drop boundary) from thermodynamic relationships[24] , and u_{Tj} is the mean molecular velocity crossing a plane in one direction[13] .

Throughout this study, a thermodynamic state will be called 'supercritical' if either the pressure or the temperature at those conditions exceeds the critical point. Indeed, what differentiates the subcritical from the supercritical regime is the absence of a two-phase region in the latter[25] , and instead there is only a single-phase region; for a detailed discussion see Harstad and Bellan[14] .

4.1 MODEL VALIDATION

One issue in exercising this fundamental model is the knowledge of the value of the thermal diffusion coefficient(s) which are generally unknown. Experimentally determined values are scarce (see Hirshfelder et al.[25] and Chapman and Cowling[26]) even for low pressures, and measurements or calculations at high pressures are very scant. For the LOX/H_2 system, a value chosen from the list of Chapman and Cowling[26] is adopted. For heptane/nitrogen Harstad and Bellan[13] have used the high-temperature (i.e. 745 K) data of Nomura et al.[16] in the pressure range of 0.1 - 2 MPa to determine approximately the value of the thermal diffusion factor for heptane/nitrogen: $\alpha_{IK} = 0.1$. The simulations were performed for nominal initial conditions (superscript 0) matching the experimental data: $R^0_d = 0.35$ mm, drop-boundary temperature $T^0_{d,b} = 300$ K and far field conditions (located at $R^0_e = 4$ mm) specified consistent with those of the experiments. Although it was obvious that $\alpha_{IK} = 0.1$ fits only approximately the data, reasons for this situation were attributed to the influence of the suspending fiber in the experiment, the level of microgravity that might still have allowed buoyancy effects and the inherent dependency of α_{IK} on (p, T, Y_α). Despite this approximate fit, further simulations performed with $\alpha_{IK} = 0.1$ yielded very encouraging results. Listed in Table 1 is a comparison of the slope, K, of d^2 with t for a variety of pressures and temperatures encompassing all the data of Nomura et al.[16] and also the data of Sato[27] . Comparison with Sato's[27] data were performed for $R^0_d = 0.5$ mm, which is the drop size used in the experiment. Generally, the numerical results approximate the $d^2(t)$ experimental variation (not shown) fairly well, and the agreement in the value of K (Table 1) is very good considering that experimental error bars were not available. Noteworthy, setting $\alpha_{BK} = 0.1$ lead to significant departures of the simulation results from the data. This, together with other results for LOX/H_2 indicate that Soret and Dufour effects should not be neglected under supercritical conditions[15] .

4.2 DROP AREA BEHAVIOR AS A FUNCTION OF TIME

As explained in the section describing the model, the value of R_s is chosen to be that of the maximum density gradient location such as to correspond to optical observations and to the subcritical identification of the phase change surface.

4.2.1 Heptane drops in nitrogen: time history of d^2

Under atmospheric conditions, the variation of d^2 with t is linear and K is termed the evaporation constant. Illustrated in Fig. 1 are d^2 and K at an ambient temperature of 470 K (Figs. 1a and 1b), and of 1000 K (Fig. 1c and 1d). At low ambient temperature, the heat up time increases with pressure (see Fig. 1a), and for the larger pressure, the drop even increases in size due to the decrease in the drop density (see more on this below). Past the initial heat up time whose duration increases with pressure, the results show a nearly linear $d^2(t)$ variation and a monotonic increase in the drop lifetime with increasing pressure. The global non-linear variation of $d^2(t)$ at larger than atmospheric pressures is documented in Fig. 1b. In contrast with the variation at atmospheric pressure, where the initial heat up time is short with respect to the drop lifetime and K is globally constant, for larger pressures K is an increasing function of time and a decreasing function of pressure. Parallel results at high temperature (Fig. 1c) display a different variation. Whereas the linearity of $d^2(t)$ at atmospheric pressure and the non linear behavior at larger pressure is still observed, the heat up time and the drop lifetime have a non-monotonic variation with pressure, with a maximum lifetime reached in the interval 2 - 4 MPa, encompassing the critical pressure of heptane. Fig. 1c qualitatively duplicates the results in Fig. 5f of Nomura et al.[16] , which were obtained for the same species and in the same range of pressures, but for a larger drop and at somewhat lower temperatures (648 - 661

K). The value of K corresponding to the results of Fig. 1c is displayed in Fig. 1d and, as expected, it exhibits a larger magnitude than at the lower temperature. At atmospheric pressure, K is nearly constant, however, for the other pressures K is a much stronger function of time than at lower temperature (Fig. 1b). The change in the magnitude of K (Fig. 1d) for $p > 0.1$ MPa leads to a maximum lifetime (Fig. 1c) at an intermediate pressure value. At large times, K is an increasing function of pressure, whereas at the subcritical temperature with respect to the drop species it was a decreasing function of pressure.

4.2.2 LOX drops in hydrogen: time history of d^2

Results illustrating the R_s^2 variation with t and the corresponding slope of these curves are presented in Figs. 2a and 2b, respectively. Because the value of R_s is available only at output points rather than at all time steps (there may be hundreds of time steps between output points), plotted in Fig. 2a are both the output points values as symbols, and n^{th} order polynomial fits as curves representing the best fit of the output points for each of the runs. Early time output points which could not be incorporated into a polynomial fit, representing transients due to initial conditions, are not shown; these include a substantial part of the drop heat up time. The fitted curves appear almost linear, despite the lack of any assumption that may lead to such behavior. Depicted in Fig. 2b is the value of K for all curves displayed in Fig. 2a. As expected, at 1.5 MPa the value of K is nearly constant, following closely the d^2- law behavior. However, K is not strictly constant, in agreement with the above results for heptane drops in nitrogen, showing that departures from the d^2 linear behavior with t occur even for pressures closely in excess of atmospheric. For larger pressures, departures from the linear d^2 behavior are evident, with the largest departure occurring around the LOX critical point where K cannot be considered constant even for a limited time range. In agreement with the heptane/nitrogen experimental results of Nomura et al.[16] and Sato[27] , K has a non-monotonic variation with pressure, first increasing, then decreasing around the critical point, and finally increasing again to reach an almost asymptotic behavior. Sato[27] found a maximum of the drop lifetime (i.e. a minimum in the value of K) in the supercritical vicinity of the critical pressure, similarly to the present predictions.

Note that, whereas the area versus time exhibits a negative curvature for C_7H_{16} drops in N_2, it displays a positive curvature for LOX drops in H_2.

4.3 REDUCED PRESSURE AND TEMPERATURE: C_7H_{16} DROPS IN N_2

As discussed in the Introduction, a common assumption of many models is that the drop boundary coincides with the mixture critical point. This statement includes actually two assumptions: (1) that the critical point is reached at a location in the mixture, and (2) that the location where the critical point is reached coincides with the drop boundary. The set of simulations discussed above offers an opportunity to evaluate this assumption because it encompasses supercritical and subcritical pressures and temperatures with respect to the pure species.

Shown in Fig. 3 is the low (subcritical with respect to heptane) temperature behavior at 0.1 MPa. The plots represent the spatial variation of ρ (Fig. 3a), p_r (Fig. 3b), T_r (Fig. 3c) and α_D (Fig. 3d) at several time stations. The density profiles show a fluid drop whose size is continuously reduced, but whose density remains constant and consistent with that of a liquid, as is should be at atmospheric pressure; outside the drop, the density magnitude is that of a gas, and therefore does not appear on the graph scale which has been chosen purposefully to be the same for Figs. 3a, 4a, 5a and 6a (see below). The pressure is everywhere subcritical, whereas the temperature is supercritical for the pure nitrogen (both air and nitrogen at atmospheric conditions are in the supercritical regime) and remains consistently subcritical in the drop as its temperature does not exceed the boiling point of heptane. Since the temperature is the thermodynamic variable that relaxes first, due to the very large effective Lewis number (see Harstad and Bellan[28]), the extent of the radial domain for Fig. 3c is enlarged compared to Figs. 3a and 3b, in order to display the full profiles. The mixture of heptane and nitrogen outside of the drop is nearly ideal ($\alpha_D \simeq 1$), as expected at atmospheric pressure, and α_D reaches a minimum at the drop boundary, a feature prevailing in all of the results presented below. Therefore the physical picture corresponds to the well known process of evaporation at low pressure and temperature. When the ambient temperature is increased, but the pressure remains atmospheric, the basic characteristics of the situation are unchanged with the exception of the time

scale which becomes much shorter. The illustrations in Figs. 4a - 4d parallel those of Figs. 3a - 3d.

The physical picture changes however appreciably once the pressure is increased. Displayed in Figs. 5a - 5d are equivalent plots to those of Figs. 3a - 3d, but at a pressure of 5 MPa. Instead of the constant density, we witness here a continuously decreasing density with time (Fig. 5a) resulting from the nitrogen dissolving in the heptane drop and from the drop heating. Note that, although the density decreases inside the drop, it remains nearly uniform at all times. Throughout the drop lifetime, the pressure is supercritical inside the drop and subcritical (except for the initial condition) outside the drop (Fig. 5b), with the opposite occurring for the temperature (Fig. 5c). This is to say that in both sides of the drop boundary, the mixture is supercritical, but there is a different supercritical state. The remarkable fact is that although there is no phase change, the fluid properties on each side of the boundary are very distinct, and the characteristics of the internal liquid-like and external gas-like fluids are maintained over the drop lifetime. This is in contrast to LOX drops in H_2 (see Harstad and Bellan[29]) where profiles of the primitive variables are smooth, with no jumps, this being due to the high solubility of H_2 in LOX. The indication that the critical point is not reached anywhere in the field is emphasized by the mass diffusion factor shown in Fig. 5d, which does not reach a null value (a necessary condition for being at the critical point; see eq. 12), although the mixture exhibits considerable departures from ideality.

At far-field supercritical temperature and pressure (Figs. 6a -6d), the features encountered at subcritical (with respect to the fuel) ambient temperature are maintained, with the difference that now the density not only decreases with time, but exhibits substantial non-uniformities inside the drop (Fig. 6a). Again, the mixture on the two sides of the drop boundary is supercritical (Figs. 6b and 6c), a conclusion reinforced by the plots of α_D in Fig. 6d, which show greater departures from non-ideality than at far field subcritical temperatures, but remain far from the null value.

Compared to the LOX/H_2 system, the heptane/nitrogen mixture stays further away from the critical point, since values of α_D as low as 0.25 were encountered[15] for LOX/H_2 at an ambient pressure of 6MPa and temperature of 1000 K. Nevertheless, even at these ambient conditions close to the critical point, the LOX drop boundary never reached the critical state. With increasing ambient pressure, the state arbitrarily near the drop boundary moved further away from the critical point. Therefore, the studies of these two systems of species do not support the assumption that the critical point is reached anywhere between the drop center and the far field, or that the drop boundary coincides with the critical mixture condition. When either the far-field pressure or the far-field temperature are supercritical, the mixture on both sides of the drop boundary is supercritical, but, depending on the solubility of the species, may be at a different supercritical state corresponding to the fluid properties of that mixture. And, as discussed above, in the context of thermodynamic modeling it is only appropriate to discuss the conditions at R_d^- and R_d^+ since the conditions at R_d cannot be readily defined if there is a jump at R_d.

4.4 VARIATION OF d^2 AS A FUNCTION OF DROP SIZE AND PRESSURE

One of the important results of the atmospheric drop evaporation theory is that K is constant and independent of drop size, being function mainly of the fuel properties. This result is based on the quasi-steady state theory yielding the well-known d^2 law. Figures 1 - 3 show that K is no longer constant at high pressures. The question then arises as to the dependence of K on the drop size at high pressures. To investigate this aspect, K is plotted for heptane drops in Fig. 7 as a function of $t/(d^0)^2$ for three disparate drop sizes at 0.1, 2 and 5 MPa. At atmospheric pressure, we recover the classical result of independence of drop size and near constancy for K. At 2 and 5 MPa, the values of K do not coincide during the initial heat up time, however, this result may also be influenced by the initial conditions which although nominally the same, may be numerically somewhat different (see Harstad and Bellan[13] for a discussion on this topic). The remarkable result is the coincidence of K after this initial transient, at a time when each of the drops have lost only 9% of their initial mass (not shown). This high pressure result is not predictable from simple mathematical manipulations of the equations, and must await a thorough explanation. From these limited simulations, the indication is that on the scale $t/(d^0)^2$, the solution is self-similar in a parameter proportional to the drop radius squared. That is, although the quasi-steady assumption that is one of the basis of the d^2 law does not hold, rendering K variable (here increasing) with time instead of constant, in this range of

drop sizes covering more than one order of magnitude, and in this range of pressures encompassing both subcritical and supercritical pressures with respect to the drop species, K is only function of pressure at fixed temperature.

From this, necessarily limited, study it can be concluded that the large drops studied under microgravity conditions are not only of academic interest, but might be relevant to the study of small drops encountered in high pressure, power producing devices. However, we note that the most important difference between single-drop microgravity experiments and conditions in practical systems may be the fact that drops are isolated in the experiments and interacting in reality.

4.5 RELAXATION TIME SCALE AT SUPERCRITICAL PRESSURES

The relaxation time scale at the drop boundary measures how fast molecules leave the boundary or come to it from the surrounding field. Under atmospheric, evaporative conditions, the relaxation time measures the evaporation time scale. Since at supercritical pressures there is no longer a surface, and the latent heat is null, the concept of evaporation no longer applies. However, there is still a mass flux from the drop boundary and it can be calculated in a general manner employing eq. 13; Harstad and Bellan[13] have called this mass flux 'the emission rate' to enable the utilization of a terminology including both subcritical and supercritical situations. Equation 13 states that the net mass flux is the difference between the flux leaving the boundary and that coming to the boundary, and the time scale of the process is determined by the values of the accommodation coefficients, α_{aj}. Under subcritical conditions, a common assumption is that this relaxation time is very small, leading to quasi-steadiness of this process with respect to all other time scales. This small relaxation time renders the set of equations very stiff, and thus difficult to solve. This difficulty, together with the uncertainties associated with the values of the accommodation coefficients provide the incentive to neglect eq. 13 and find a simpler thermodynamic statement, such as the equality of the fugacities at the boundary, as a replacement.

The assumption of very small relaxation time was investigated under the atmospheric condition by Bellan and Summerfield[30] , and more recently by Miller et al.[31] , and it was found to hold reasonably well for drops of diameter larger than 50 μm; for smaller drops, the assumption proved to be unreliable. Since as discussed in the Introduction, the hypothesis of the small relaxation time is used in some models of high pressure drops, we examined its validity by varying the accommodation coefficients from the baseline values $\alpha_{a1} = \alpha_{a2} = 1$ as follows: (1) $\alpha_{a1} = \alpha_{a2} = 0.1$, (2) $\alpha_{a1} = \alpha_{a2} = 3$, (3) $\alpha_{a1} = \alpha_{a2} = 10$, (4) $\alpha_{a1} = 10, \alpha_{a2} = 3$. For heptane drops having $R_d^0 = 6 \times 10^{-3}$ cm and $R^{si,0} = 0.05$ cm, it was found that d^2 and K coincide for all five conditions, indicating that indeed the relaxation time is small. The values $\alpha_{a1} = 10, \alpha_{a2} = 3$ were also used for heptane drops having $R_d^0 = 2 \times 10^{-3}$ cm and $R^{si,0} = 0.017$ cm, and the results were compared with those obtained for $\alpha_{a1} = \alpha_{a2} = 1$; the curves d^2 and K versus $t/(d^0)^2$ exhibited again complete coincidence. In fact, when plotted versus $t/(d^0)^2$, the K curves coincide for the two drop sizes and the different accommodation coefficients (a total of seven simulations) over the entire drop lifetime with the exception of the short drop-heat-up duration; this indicates that on that scale, the process of drop disappearance is only pressure dependent.

5 CONCLUSIONS

A numerical study of fluid drop behavior has been conducted using a model that is valid at all pressures. This model is based on fluctuation-dissipation theory, which is consistent with non-equilibrium thermodynamics, and leads to the most general form of the flux equations, including the Soret and Dufour effects. To close the system, conservation equations are completed by the equation of state, valid for all pressures. The traditional transport coefficients used in the simulations were calculated as functions of the thermodynamic variables; the thermal diffusion factor, which is the new transport coefficient introduced by the Soret and Dufour effects, was chosen according to the value determined during the previous validation study. The drop boundary conditions were based on the conservation of mass, energy and species across the boundary, with no assumption made about the occurrence of quasi-steadiness in mass transfer to/from the boundary. Calculated after obtaining the solution, the drop boundary was identified with the location of the maximum density change because of the relevance to optical measurements. It was shown that, consid-

ering that experimental error bars were not available, this model reproduces very favorably heptane drop evolution in nitrogen under microgravity conditions.

The linear dependency of the diameter squared versus time is approximately encountered only at atmospheric pressure; this holds both for heptane drops in nitrogen and for LOX drops in H_2 Heptane/nitrogen simulations performed for an extensive set of initial conditions show that whereas the drop lifetime increases monotonically with pressure at subcritical (with respect to the pure drop species) temperatures, at supercritical (also with respect to the pure drop species) temperatures a maximum is reached. This result is confirmed by existing microgravity data. As the pressure increases, the slope of the diameter squared, K, becomes an increasing function of time; this slope progressively increases with pressure at subcritical far-field temperatures, however, at supercritical temperatures a maximum is reached. Results obtained for different drop diameters spanning more than an order of magnitude display the traditional independence of K on the drop size at atmospheric pressure when time is scaled as $t/(d^0)^2$. As the pressure is increased, the early part of $K(t)$ (corresponding both to the initial drop heating and to possible transients arising from initial conditions that are nominally the same but perhaps numerically somewhat different; see explanation in Harstad and Bellan[13]) is drop size dependent, however, during the majority of the drop lifetime corresponding to more that 90% of the mass, the values of K are again size independent. This indicates that the solution is self-similar in a variable proportional to the drop radius squared; this fact cannot be predicted from simple scrutiny of the equations and should be further investigated. However, whereas the slope of the drop diameter squared versus time has a negative curvature for heptane/nitrogen, it has a positive curvature for LOX/H_2. This indicates that results from studies of a species system should not be simply extrapolated to other systems of species.

Independent of the binary species system, it is found that at supercritical pressures, the critical point is never reached arbitrarily close to the drop boundary. Instead, two supercritical states, each portraying the specific mixture, coexist on the two sides of the drop boundary. Therefore, these results do not support previous models based on the assumption that the critical point is attained in the domain, and that it is reached at the drop boundary.

The effect of the relaxation time scale at the drop boundary was found to be negligible even for relatively small drops. Therefore the assumption of quasi-steadiness in the mass fluxes to/from the drop surface appears to be valid within the range of drop sizes investigated. From the practical viewpoint, this finding could be important, if of general validity, and used judiciously could simplify CFD calculations.

Further work on this topic focuses on the development of models for the calculation of high-pressure transport coefficients, such as diffusivities[32] and thermal diffusion factors. Also of interest is the extension of the binary species results to systems of several species. The multicomponent species theory is available[13] , and the determination of high-pressure transport coefficients should enable such simulations.

ACKNOWLEDGMENT

This research was conducted at the Jet Propulsion Laboratory, California Institute of Technology, under sponsorship from the National Aeronautics and Space Administration, the Glenn Research Center at Lewis Field, with Dr. Daniel L. Bulzan as technical contract monitor and from the Marshall Space Flight Center, with Mr. Klaus Gross as technical monitor. Their continuing interest and support are greatly appreciated.

[1] Bellan, J., Supercritical (and Subcritical) Fluid Behavior and Modeling: Drops, Streams, Shear and Mixing Layers, Jets and Sprays, *Prog. Energy Combust. Sci.*, 26(4-6): 329-366 (2000)

[2] Shuen, J-S., Yang, V. and Hsiao, G. C., Combustion of liquid-fuel droplets in supercritical conditions, *Combust. Flame*, 89: 299-319 (1992)

[3] Yang, V., Lin, N. N. and Shuen, J-S., Vaporization of liquid oxygen (LOX) droplets in supercritical hydrogen environments, *Comb. Sci. and Tech.*, 97: 247-270 (1994)

[4] Hsiao, G. C., Yang V. and Shuen, J. S., Supercritical vaporization and dynamics of liquid oxygen (LOX) droplet in hydrogen stream, AIAA 95-0383, 33rd Aerospace Sciences Meeting, Reno, NV, 1995

[5] Haldenwang, P., Nicoli, C. and Daou, J., High pressure vaporization of LOX droplet crossing the critical condition, *Int. J. Heat Mass Transfer*, 39(16): 3453-3464 (1996)

[6] Umemura, A., Supercritical liquid fuel combustion, *Proc. of the Comb. Inst.*, 21: 463-471 (1986)

[7] Curtis and Farrell, P. V., Droplet vaporization in a supercritical microgravity environment, *Acta Astronautica*, 17(11/12): 1189-1193 (1988)

[8] Chiang, C. H. and Sirignano, W. A., Axisymmetric vaporizing oxygen droplet computations, AIAA 91-0281, 29th Aerospace Sciences Meeting, Reno, NV, 1991

[9] Curtis, E. W. and Farrell, P. V., A numerical study of high-pressure droplet vaporization, *Combust. Flame*, 90: 85-102 (1992)

[10] Jia, H. and Gogos, G., Investigation of liquid droplet evaporation in subcritical and supercritical gaseous environments, *Journal of Thermophysics and Heat Transfer*, 6(4): 738-745 (1992)

[11] Jia, H. and Gogos, G., High pressure droplet vaporization; effects of liquid-phase solubility, *Int. J. Heat Mass Transfer*, 36(18): 4419-4431 (1993)

[12] Umemura, A. and Shimada, Y., Linear acoustic characteristics of supercritical droplet vaporization, *Proc. of the Comb. Inst.*, 27: 2659-2665 (1998)

[13] Harstad, K. and Bellan, J, An All-Pressure Fluid Drop Model Applied to a Binary Mixture: Heptane in Nitrogen, *Int. J. of Multiphase Flow*, 26(10): 1675-1706 (2000)

[14] Harstad, K. and Bellan, J., Evaluation of commonly used assumptions for isolated and cluster heptane drops in nitrogen at all pressures, *Combustion and Flame*, 127 (1 – 2): 1861-1879 (2001)

[15] Harstad, K. and Bellan, J., The D^2 Variation for Isolated LOX Drops and Polydisperse Clusters in Hydrogen at High Temperature and Pressures, *Combustion and Flame*, 124: 535-550 (2001)

[16] Nomura, H., Ujiie, Y., Rath, H. J., Sato, J. and Kono, M., Experimental study on high pressure droplet evaporation using microgravity conditions, *Proc. of the Comb. Inst.*, 26: 1267-1273 (1996)

[17] Keizer, J., *Statistical thermodynamics of nonequilibrium processes*, Springler-Verlag, New York, 1987

[18] Sarman, S. and Evans, D. J., Heat flux and mass diffusion in binary Lennard-Jones mixtures, *Phys. Rev.*, A45(4): 2370-2379 (1992)

[19] Reid, R. C., Prausnitz, J. M. and Polling, B. E., *The properties of gases and liquids*, 4th Edition, McGraw-Hill Book Company, 1987

[20] Harstad, K., Miller, R. S. and Bellan, J., Efficient high pressure state equations, *AIChE J.*, 43(6): 1605-1610 (1997)

[21] Peng, D-Y. and Robinson, D. B., A rigorous method for predicting the critical properties of multicomponent systems from an equation of state, *AIChE J.*, 23(2): 137-144 (1977)

[22] Reamer, H. H. and Sage, B. H., Phase equilibriums in hydrocarbon systems. Volumetric and phase behavior of the n-decane-CO2 system, *J. Chem. Eng. Data*, 8(4): 508-513 (1963)

[23] Kay, W. B., Liquid-vapor phase equilibrium relations in the ethane-n-heptane system, *Ind. Eng. Chem*, 30: 459-465 (1938)

[24] Prausnitz, J., Lichtenthaler, R. and de Azevedo, E., *Molecular thermodynamics for fluid-phase equilibrium*, Prentice -Hall, Inc, 1986

[25] Hirshfelder, J. O., Curtis, C. F. and Bird, R. B., *Molecular Theory of Gases and Liquids*, John Wiley and Sons, Inc, 1964

[26] Chapman, S. and Cowling, T. G., *The Mathematical Theory of Nonuniform Gases*, Cambridge University Press, Cambridge, 1970.

[27] Sato, J., Studies on droplet evaporation and combustion in high pressures AIAA 93-0813, 31st Aerospace Sciences Meeting Jan. 11-14, Reno, NV (1993)

[28] Harstad, K. and Bellan, J, The Lewis Number Under Supercritical Conditions, *Int. J. Heat and Mass Transfer*, 42: 961-970 (1999)

[29] Harstad, K. and Bellan, J., Isolated Liquid Oxygen Drop Behavior in Fluid Hydrogen at Rocket Chamber Pressures, *Int. J Heat and Mass Transfer*, 41: 3537-3550, 1998

[30] Bellan, J and Summerfield, M., Theoretical examination of assumptions commonly used for the gas phase surrounding a burning drop, *Combust. and Flame*, 33: 107-122 (1978)

[31] Miller, R. S., Harstad, K. and Bellan, J., Evaluation of Equilibrium and Non-Equilibrium Evaporation Models for Many Droplet Gas-Liquid Flow Simulations, *Int. J. of Multiphase Flow*, 24: 1025-1055 (1998)

[32] Harstad, K. and Bellan, J., High Pressure Binary Mass Diffusion Coefficients for Combustion Engineering Applications and Sensitivity Study for Drops in Zero Gravity, submitted to the *Proc. of the Combustion Institute*, 29, 2001

p_e, MPa	T_e, K	$K_{\mu g}$	K_{ap}	$K_{ap}/K_{\mu g}$
0.1	470	0.116 (Nom)	0.135	1.16
0.1	655	0.306 (Nom)	0.280	0.92
0.1	745	0.390 (Nom)	0.350	0.90
0.5	470	0.117 (Nom)	0.135	1.15
0.5	655	0.356 (Nom)	0.320	0.90
0.5	745	0.437 (Nom)	0.390	0.89
1.0	470	0.138 (Nom)	0.135	0.98
1.0	655	0.424 (Nom)	0.330	0.78
2.0	445	0.097 (Sat)	0.0935	0.97
2.0	452	0.096 (Nom)		
2.0	655	0.475 (Nom)	0.360	0.76
2.0	745	0.4 - 1.7 (Nom)	0.450	—
5.0	495	0.2 - 0.13 (Nom)	0.140	0.70 - 1.08

Table 1: Maximum regression rate of the maximum density gradient location, K in mm^2/s, obtained from the current model (ap), Nomura et al.'s, 1996 (Nom) and Sato's, 1993 (Sat). In the simulations T_d^0 = 300 K and d^0 = 0.7 mm, while Nomura et al.'s d^0 was 0.6 - 0.8 mm and Sato's was 1mm.

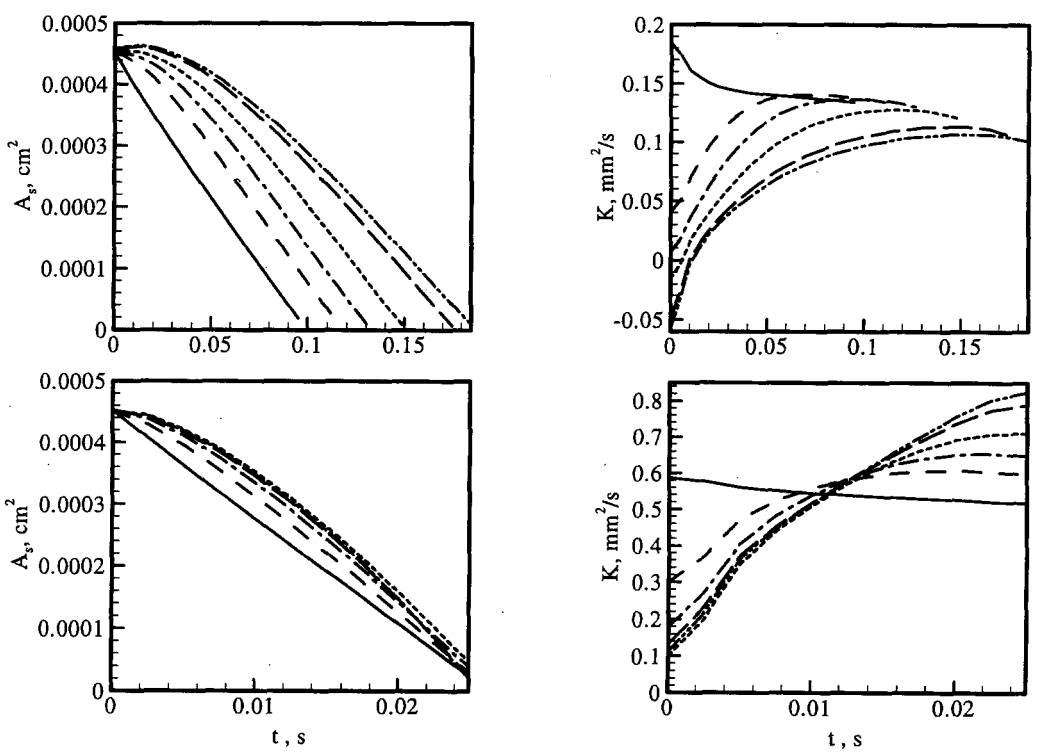

Figure 1. Variation of an isolated C_7H_{16} drop boundary area, A_s, and its derivative, K, with time for various pressures, at subcritical (Figs. 1a and 1b), and supercritical (Figs. 1c and 1d) ambient temperatures in N_2. For all simulations $R_d^0 = 6 \times 10^{-3}$ cm, $R^{si,0} = 5 \times 10^{-2}$ cm and $T_d^0 = 325$ K. For Figs. 1a and 1b, $T_e = 470\ K$. For Figs. 1c and 1d, $T_e = 1000\ K$. In all figures, the legend is as follows: 0.1 MPa (——), 0.5 MPa (– – –), 1 MPa (– · – · –), 2 MPa (- - -), 4 MPa (— —), and 5 MPa (– · · – · · –).

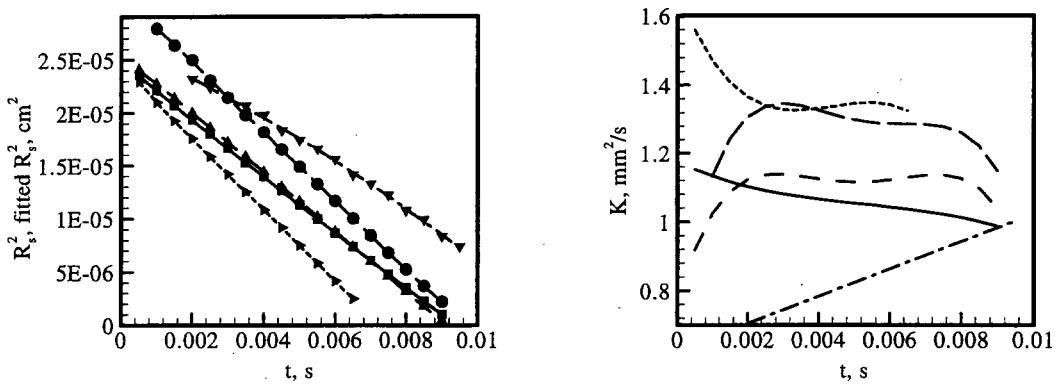

Figure 2. (2a) Variation of R_s^2 with t for isolated LOX drops in H_2. The initial drop radius was $R_d^0 = 5 \times 10^{-3}$ cm, $T_d^0 = 120$ K and $T_e = 1000\ K$ in all simulations. Symbols correspond to values obtained at the output points, whereas the curves correspond to an nth order, best polynomial fit. 1.5 MPa: simulation output ■, 4th order polynomial fit (——); 3 MPa: simulation output ▲, 5th order polynomial fit (– – –); 6 MPa: simulation output ▼, 2nd order polynomial fit (– · – · –); 10 MPa: simulation output ►, 4th order polynomial fit (- - -); 20 MPa: simulation output •, 5th order polynomial fit (— —). (2b) Variation of the slope of the fitted $R_s^2(t)$, K, with time. 1.5 MPa (——); 3 MPa (– – –); 6 MPa (– · – · –); 10 MPa (- - -); 20 MPa (— —).

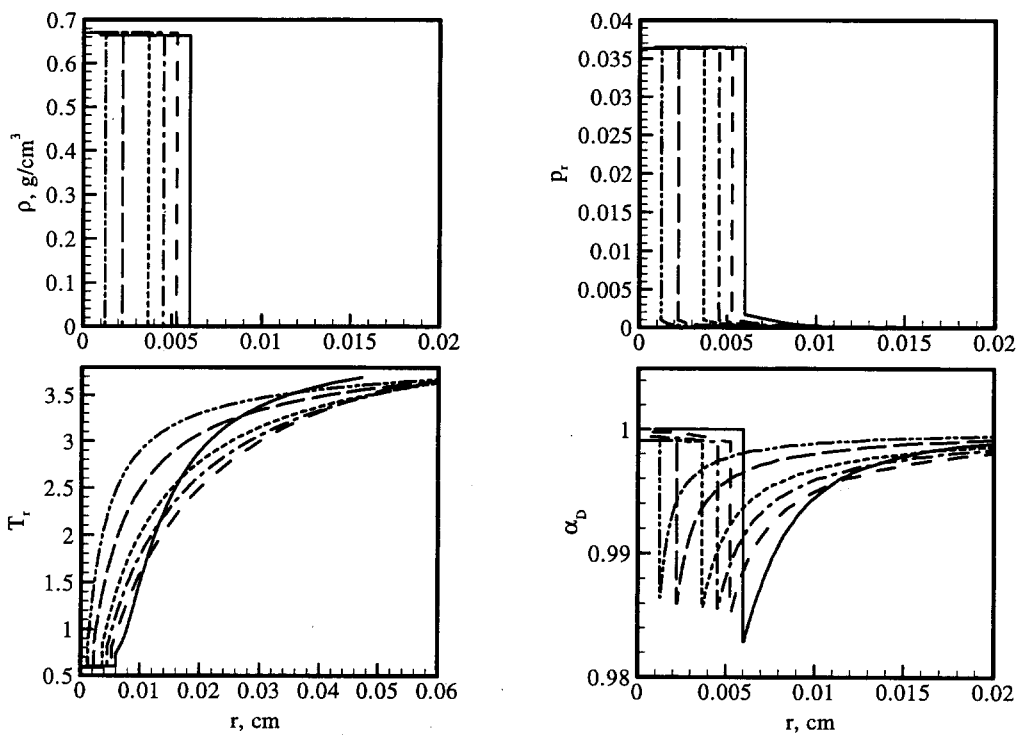

Figure 3. Drop evolution at 0.1 MPa and $T_e = 470\ K$ for drops having: $R_d^0 = 6\times10^{-3}$ cm, $R^{si,0} = 5\times10^{-2}$ cm and $T_d^0 = 325$ K. ρ, p_r, T_r and α_D at times: 0 s (——), 2×10^{-2} s (– – –), 4×10^{-2} s (– · – · –), 6×10^{-2} s (- - -), 8.5×10^{-2} s (— —), and 9.5×10^{-2} s (– · · – · · –).

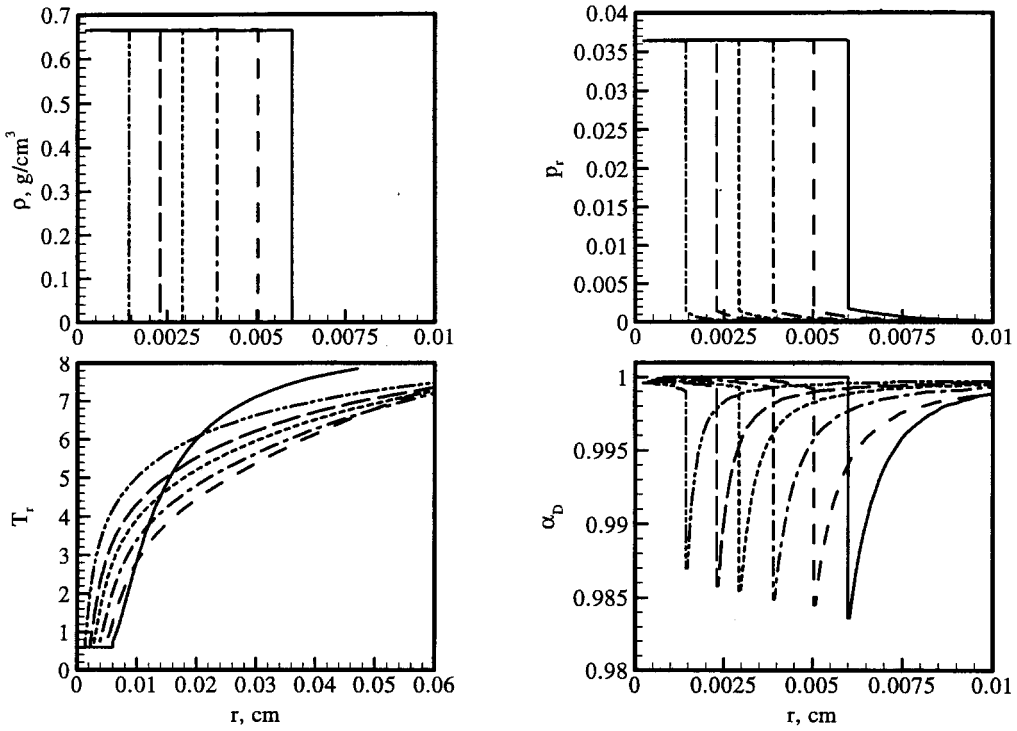

Figure 4. Drop evolution at the same initial conditions as in Fig. 3 except that $T_e = 1000\ K$. Legend: 0 s (——), 7.5×10^{-3} s (– – –), 1.5×10^{-2} s (– · – · –), 2×10^{-2} s (- - -), 2.25×10^{-2} s (— —), and 2.5×10^{-2} s (– · · – · · –).

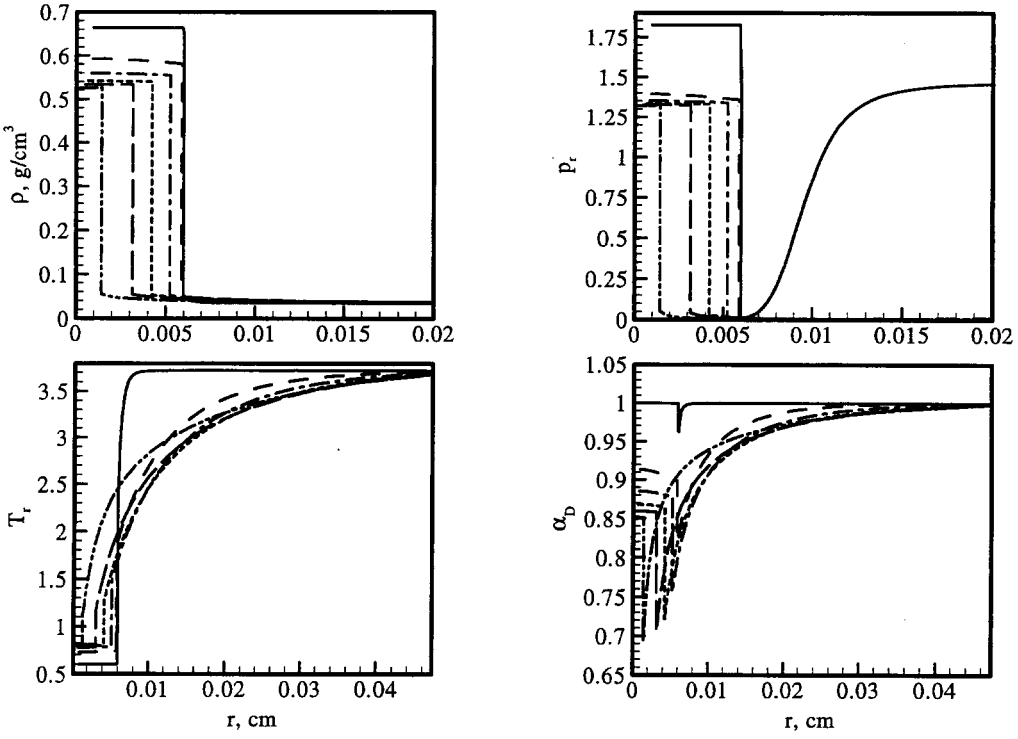

Figure 5. Drop evolution at the same initial conditions as in Fig. 3 except that 5 MPa. Legend: 0 s (——), 4×10^{-2} s (– – –), 6×10^{-2} s (– · – · –), 1.2×10^{-1} s (- - -), 1.5×10^{-1} s (— —), and 1.8×10^{-1} s (– · · – · · –).

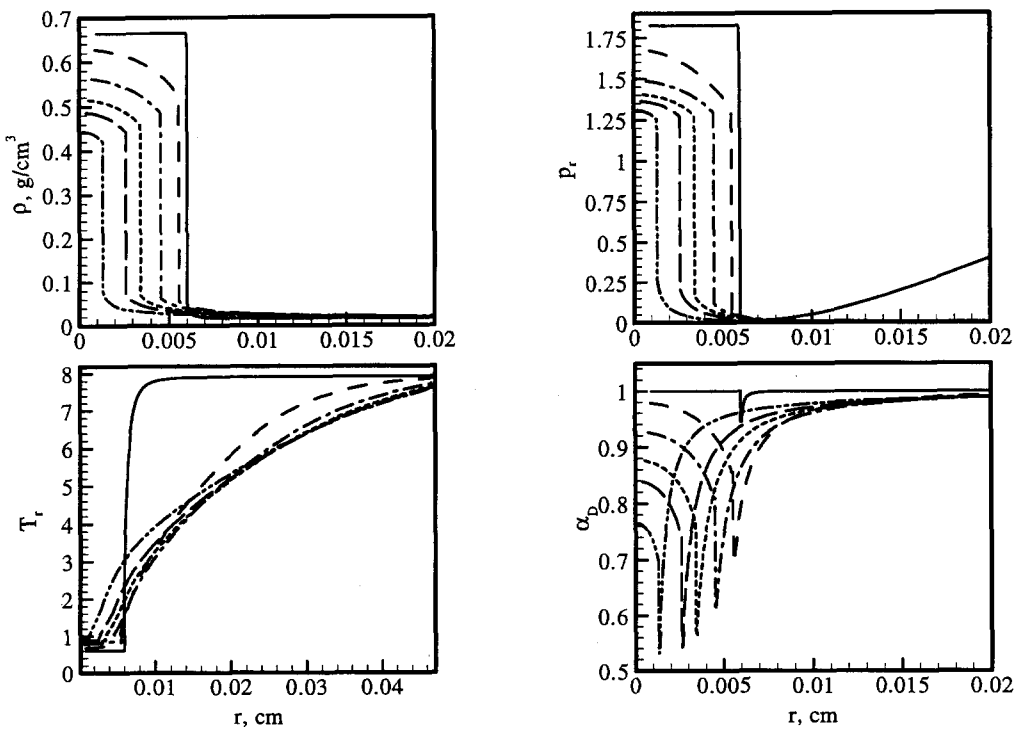

Figure 6. Drop evolution at the same initial conditions as in Fig. 5 except that $T_e = 1000\ K$. Legend: 0 s (——), 7.5×10^{-3} s (– – –), 1.5×10^{-2} s (– · – · –), 2×10^{-2} s (- - -), 2.25×10^{-2} s (— —), and 2.5×10^{-2} s (– · · – · · –).

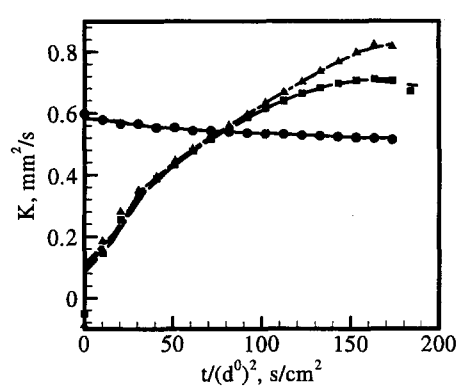

Figure 7. Dependence of K on the drop size and pressure: C_7H_{16} drops in N_2. Three drop sizes and pressures are considered, as follows: $R_d^0 = 2 \times 10^{-3}$ cm ($R^{si,0} = 1.7 \times 10^{-2}$ cm): 0.1 MPa (——), 2 MPa (– – –), 5 MPa (– · – · –); $R_d^0 = 6 \times 10^{-3}$ cm ($R^{si,0} = 5 \times 10^{-2}$ cm): 0.1 MPa (- - -), 2 MPa (— —), 5 MPa (– · · – · · –); $R_d^0 = 3.5 \times 10^{-2}$ cm ($R^{si,0} = 3 \times 10^{-1}$ cm): 0.1 MPa (•), 2 MPa (■), 5 MPa (▲). $T_e = 1000$ K, $T_d^0 = 325$ K.